

# Particle-Filtering-based Latent Diffusion for Inverse Problems

Amir Nazemi, Mohammad Hadi Sepanj\*, Nicholas Pellegrino\*, Chris Czarnecki\*, Paul Fieguth

Vision & Image Processing Lab, Department of Systems Design Engineering, University of Waterloo, Waterloo, Ontario, Canada (e-mails: amir.nazemi, mhsepanj, nicholas.pellegrino, cczarnecki, paul.fieguth@uwaterloo.ca)

## Abstract

Current strategies for solving image-based inverse problems apply latent diffusion models to perform posterior sampling. However, almost all approaches make no explicit attempt to explore the solution space, instead drawing only a single sample from a Gaussian distribution from which to generate their solution. In this paper, we introduce a particle-filtering-based framework for a nonlinear exploration of the solution space in the initial stages of reverse SDE methods. Our proposed particle-filtering-based latent diffusion (PFLD) method and proposed problem formulation and framework can be applied to any diffusion-based solution for linear or nonlinear inverse problems. Our experimental results show that PFLD outperforms the SoTA solver PSLD on the FFHQ-1K and ImageNet-1K datasets on inverse problem tasks of super-resolution, Gaussian deblurring and inpainting.

## 1 Introduction

In recent years, *generative* methods (Harshvardhan et al. 2020; Compton, Osborn, and Mateas 2013; Harshvardhan et al. 2020) have come into use for solving inverse problems (Rout et al. 2023b; Chung et al. 2022; Dimakis 2022). These methods make use of the prior learned by a *generative model* to best solve a given class of inverse problems (Shah and Hegde 2018; Bertero, Boccacci, and De Mol 2021). In particular, the approach of using generative models offers a substantial improvement compared to conventional deterministic methods (Lunz, Öktem, and Schönlieb 2018) due to their inherent ability to *sample* from the *posterior-distribution*, thereby yielding more plausible estimates (Fieguth 2010).

From the family of generative models, diffusion models (Sohl-Dickstein et al. 2015; Croitoru et al. 2023; Song et al. 2020), further introduced in Preliminaries, have emerged as a compelling framework. Indeed, models such as DPS (Chung et al. 2022), PSLD (Rout et al. 2023b), Soft Diffusion (Daras et al. 2023), Cold Diffusion (Bansal et al. 2024), STSL (Rout et al. 2023a), and P2L (Chung et al. 2023) have demonstrated impressive performance. While these methods show promise, actual usage and performance is not robust enough. For example, in Figure 2, different random initializations lead to substantially different results,

\*These authors contributed equally.

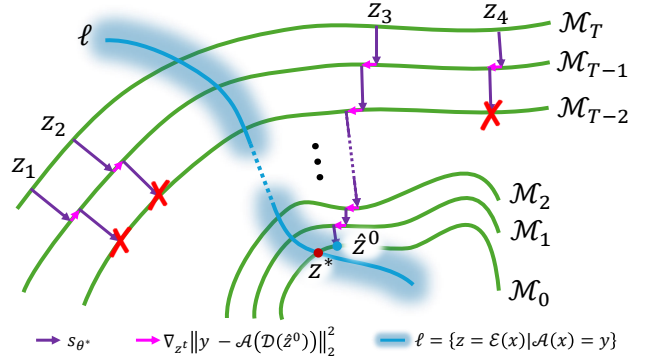


Figure 1: In the proposed PFLD method, multiple random samples,  $z_l$ , in the latent space of a diffusion model act as particles. Starting from an outer manifold,  $\mathcal{M}_T$ , indistinguishable from the space of random noise, these particles progress through steps of reverse diffusion (via  $s_{\theta^*}$ ) towards  $\mathcal{M}_0$ , a manifold corresponding to noise-free images. The line  $\ell$  corresponds to the set of plausible solutions, all of which map to the measurement,  $y$ , through the forward process  $\mathcal{A}$ . Particles are also guided towards  $\ell$  through a gradient term,  $\nabla_{x^t} \|y - \mathcal{A}(\mathcal{D}(\hat{z}_l^0))\|_2^2$ , based on intermediate estimates,  $\hat{z}_l^0$ , of where the particle will be at the end of reverse diffusion. Particles farther from  $\ell$ , destined be far from the ground truth solution,  $z^*$ , at the end of reverse diffusion, are pruned (marked with a red  $\times$ ). A final singular particle reaches  $\mathcal{M}_0$  producing the final estimated solution,  $\hat{z}^0$ .

several of which are poor. These methods make no explicit attempt to explore the solution space and are highly sensitive to initialization.

This work presents an extension to diffusion-based methods by incorporating a *particle filter* (Djuric et al. 2003) to better explore the solution space in the early stages of solving the reverse stochastic differential equation (SDE), resulting in reliably high-quality estimates. Briefly, particle filters operate by sampling a given domain at many positions (i.e., many particles), in this case, offering improvements in the *exploration* of the solution space. Iteratively, particles are compared and selected based on their relative “fitness” in solving the given problem.

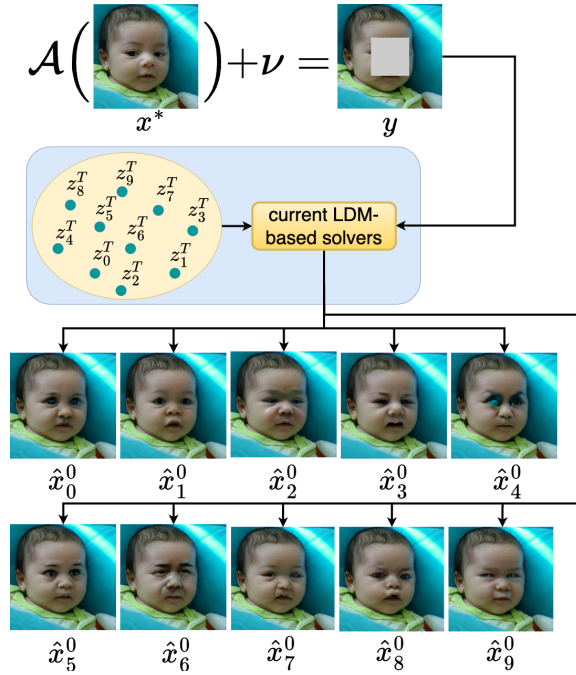


Figure 2: Ten different runs of PSLD (Rout et al. 2023b) with different initial points with different random seeds,  $z_l^T$ , produce different estimates,  $\hat{x}_l^0$ , of the ground truth image  $x^*$ . The forward model,  $\mathcal{A}$ , masks the center of  $x^*$ . The estimator only has access to the measurement  $y$  to solve the inverse problem. The image used in this figure is from the FFHQ dataset (Karras, Laine, and Aila 2019).

In this work, particles,  $z_l$ , are samples in a latent space of a diffusion model, which relate to individual solution estimates,  $\hat{x}_l$ , to the given inverse problem. Existing latent-diffusion-based methods draw only *one* sample from the Gaussian distribution to initialize the reverse SDE, from which to attempt the recovery of a noise-free sample,  $z^0$  (or  $x^0$  in the pixel-space). In contrast, the proposed method samples the latent space *many* times, through the initialization of many particles. During the process of reverse diffusion, low-scoring / poorly performing particles, likely not to lead to a compelling estimate, are pruned away, such that the number of remaining particles decreases and, on average, tend reliably towards a more optimal and visually compelling final solution. A graphical interpretation is shown in Figure 1, wherein several particles,  $z_l$ , move towards the ground truth solution,  $z^*$ . This method substantially improves the solution *robustness*, such that estimates,  $\hat{x}^0$ , are consistently close to the ground truth,  $x^*$ .

The main contribution of this paper is the creation of a general particle-filtering-based framework for solving inverse problems with diffusion models. This framework can be applied to any diffusion model to improve robustness, yielding reliably improved estimates. This framework is tested upon an existing latent diffusion model, PSLD (Rout et al. 2023b), for tasks of super-resolution, Gaussian deblurring and inpainting.

## 2 Preliminaries

Diffusion models are a type of generative model that are trained to reverse a diffusion process (Song et al. 2020; Deja et al. 2022; Cao et al. 2024). The diffusion process involves transforming a sample  $x^0 \sim p_0(x)$  through a stochastic process defined by the Stochastic Differential Equation (SDE)

$$dx = f(x, t)dt + g(t)dw,$$

where  $x$  is the input at time  $t$ , i.e.,  $x = x^0$  at  $t = 0$ . By reversing the diffusion process, diffusion models (Sohl-Dickstein et al. 2015; Song and Ermon 2020; Croitoru et al. 2023) are able to transform random samples into noise-free generated outputs.

In the formulation of pixel-space generative diffusion models, an input,  $x^0$ , is corrupted according to the SDE, which iteratively augments  $x^0$  with noise, such that finally at  $t = T$ ,  $x^T$  is indistinguishable from a sample of a Gaussian distribution (i.e., for a set of many input samples  $\{x^0\}$ , the distribution of  $\{x^T\}$  is approximately Gaussian). In contrast to pixel-space diffusion models, in *latent* diffusion models (Rombach et al. 2022), the SDE and reverse SDE are applied to the *latent* space representations,  $z$ , of a pretrained encoder,  $\mathcal{E}$ , and decoder,  $\mathcal{D}$ , pair. The method proposed in this paper is applied to PSLD (Rout et al. 2023b), a latent-space model.

### 2.1 Utilizing Diffusion Models for Solving Inverse Problems

Recently, the emergence of utilizing diffusion models as generative priors (Ho, Jain, and Abbeel 2020; Graikos et al. 2022; Deja et al. 2022) for solving inverse problems has gained prominence (Hu et al. 2024; Rout et al. 2023b; Tewari et al. 2023). In general, an inverse problem (Fieguth 2010) can be described as the task of recovering a desired unknown and underlying quantity  $x^* \in \mathbb{R}^n$  from a corrupted and noisy measurement  $y \in \mathbb{R}^m$ , generated via the forward process

$$y = \mathcal{A}(x^*) + \nu, \quad (1)$$

where  $\mathcal{A} : \mathbb{R}^n \rightarrow \mathbb{R}^m$  is a deterministic corruption process and  $\nu$  is a sample of Gaussian noise,  $\nu \sim N(0, \sigma_\nu I)$ .

Inverse problems and their diffusion-model-based solutions can be categorized based on whether the inverse problem is linear or non-linear, the forward model  $\mathcal{A}$  is known or not, and whether the pixel or latent solution space is used. If the forward process is *known*, the transformation,  $\mathcal{A}$ , can be used in the solution / optimization process. Estimates,  $\hat{x}$ , are found through

$$\hat{x} = \arg \min_x \|\mathcal{A}x - y\|. \quad (2)$$

If the forward process is *unknown*, the problem is referred to as being *blind*. Lastly, most traditional image-based inverse problems are solved in *pixel* space; however, with the inclusion of an encode-decoder architecture, it is possible to solve inverse problems in the encoded *latent space*.

In most inverse problems, such as inpainting, super-resolution, and deblurring, some information is *lost* during the forward process,  $y = \mathcal{A}(x)$ . The task then of recovering

the original information,  $x$ , from corrupted measurements,  $y$ , is inherently difficult due to the many-to-one nature of the problem, and  $\mathcal{A}^{-1}$  does not exist.

Recent advancements in generative modeling have led to notable progress in solving inverse problems. The framework proposed by (Song et al. 2020) utilizes score-based generative models with integrated data consistency constraints, achieving enhanced reconstruction quality and computational efficiency, though it requires extensive training data and involves complex score estimation. In (Chung et al. 2023), Prompt-tuning Latent Diffusion Models (P2L) were introduced, which effectively address noisy and non-linear inverse problems through posterior sampling, offering enhanced performance across various noise types but demanding significant computational resources. Most recently, (Rout et al. 2024) developed the Second-order Tweedie Sampler from Surrogate Loss (STSL), which improves sampling quality and reduces the number of diffusion steps needed, although it requires careful parameter tuning for optimal results.

A common theme across all diffusion-based methods is high sensitivity to initialization, such that results have high variability, and high computational demand, such that re-running is costly. Therefore, the development of a method or framework capable of producing high-quality results while reducing the computational load would be of substantial benefit and would represent a significant step towards practical usage of diffusion-based methods for solving inverse problem.

## 2.2 Particle filtering

In the particle filter (Gordon, Ristic, and Arulampalam 2004), particle representations of probability density are estimated via Sequential Monte Carlo (SMC) estimation (Gordon, Ristic, and Arulampalam 2004). In contrast with other linear filtering methods such as Kalman filters (Welch, Bishop et al. 1995), there is no need to impose the assumptions of linearity and Gaussian error covariance (Fieguth 2010). This freedom makes the particle filter more broadly applicable.

In this section, the general particle filtering algorithm is explained. In our proposed method, a customized particle filter method is combined with the diffusion model. Therefore, the notation of diffusion models is used.

As explained in (Arulampalam et al. 2002), the goal in the particle filter algorithm is to approximate the posterior probability density of states  $p(z^t | \{m_l\}_{l=1}^N)$ , where  $z^t$  is the state and  $\{m_l\}_{l=1}^N$  is the set of measurements, all at a given timestep  $t$ . Thus, in the particle filtering algorithm, the posterior probability density is estimated with a set of  $N$  particles and their associated weights  $\{z_l^t, w_l^t\}_{l=1}^N$  as

$$p(z^t | \{m_l\}_{l=1}^N) \approx \sum_{l=1}^N w_l^t \delta(z^t - z_l^t). \quad (3)$$

Here,  $\delta$  is the Dirac delta function and  $w_l^t$  represents the weight of each particle,  $z_l^t$ , in the particle filtering algorithm. The initial weights of all created particles are uniform, and

during the process of particle filtration, the weights are subsequently adjusted according to

$$w_l^t \propto w_l^{t-1} \frac{p(m^t | z_l^t) p(z_l^t | z_l^{t-1})}{q(z_l^t | z_l^{t-1}, m^t)}, \quad (4)$$

where,  $p(m^t | z_l^t)$  is the likelihood function defined by the measurement model,  $q(z_l^t | z_l^{t-1}, m^t)$  is the proposal distribution function that the samples can be easily generated from, and  $p(z_l^t | z_l^{t-1})$  is the probabilistic model of state evaluation.

In order to estimate the posterior probability density of states  $p(z^t | \{m_l\}_{l=1}^N)$  at time  $t$ , we need a set of  $N$  particles and weights  $\{z_l^t, w_l^t\}_{l=1}^N$ . The weights can be calculated using Equation (4). Thus, given a set of  $N$  particles  $\{z_l^{t-1}, w_l^{t-1}\}_{l=1}^N$  at time  $t-1$ , the particle filter does the following three steps (Gordon, Ristic, and Arulampalam 2004) to estimate the new set of particles and weights:

1. **Prediction:** A set of new particles are generated by sampling from  $q(z_l^t | z_l^{t-1}, m^t)$ .
2. **Updating the weights:** Given a new measurement  $m^t$ , a weight  $w_l^t$  is calculated and assigned to each particle  $z_l^t$  using equation 4. This weight  $w_l^t$  is associated with the quality of the particle  $z_l^t$  given the measurement  $m^t$ .
3. **Resampling:** Typically, after several iterations, many of the particles will have a small weight and updating these particles in each time step is costly and does not tend to impact the solution. This phenomenon is called the degeneracy problem (Doucet, Johansen et al. 2009). A solution to this problem is to do resampling with replacement from  $\{z_l^t, w_l^t\}_{l=1}^N$  using the weights  $\{w_l^t\}_{l=1}^N$  that are calculated in the previous step. Resampling favours particles that have a higher quality (measured as their weight). After resampling, the weights are reset to  $w_l^t = \frac{1}{N}$ .

The degeneracy metric  $N_d$  is related to effective sample size (Salmond 1990) and is estimated as,

$$N_d \approx \frac{1}{\sum_{i=1}^N (w_i^t)^2}. \quad (5)$$

It can be shown that  $1 \leq N_d \leq N$ . The degeneracy metric is equal to  $N$  after each resampling since the weights are set to  $\frac{1}{N}$ . A threshold  $N_{th}$  is set, for which resampling is performed if ever  $N_d \leq N_{th}$ .

## 3 Method

The proposed method, Particle-Filtering-based Latent Diffusion (PFLD), is a framework that integrates a particle filter on top of existing diffusion-based inverse problem solvers. Although this method can be applied to any existing diffusion-based method, as an example, we use PSLD (Rout et al. 2023b), a state-of-the-art (SoTA) diffusion-based method for solving inverse problems. We chose PSLD primarily because replicating the results of other SoTA is impractical; for example, at the time of writing this paper, the code for STSL was not published.

The algorithm for this proposed framework, integrated with PSLD, is shown in Algorithm 1. To be concise, we introduce a function PSLD( $\cdot$ ) to encapsulate one iteration of

the PSLD method. If the use of a method other than PSLD is desired, then  $\text{PSLD}(\cdot)$  need only be replaced with a function encapsulating one iteration of that method. A complete version of the proposed algorithm is shown and explained in the supplementary material.

The particle filter essentially ‘wraps around’ the given diffusion-based model, such that for each particle, reverse diffusion is carried-out independently. The interaction between particles occurs only during resampling and pruning. For this framework, we require a set of  $N$  particles, indexed by subscript  $l$ , each with an associated state,  $z_l^t$ , and weight,  $w_l^t$ . In PSLD, an intermediate estimate,  $\hat{z}_l^0$ , of where the particle will be at the end of reverse diffusion is generated at every time step. Note that for reverse diffusion, time steps,  $t$ , start from  $T$  and end at 0. At each time step, the reverse SDE is applied to all particles to update their states.

In PFLD, the corrupted image,  $y$ , is used as the measurement at all time steps, i.e.,  $m^t = y \forall t$ . Moreover, the likelihood PDF  $p(y|\hat{z}_l^0)$  is modeled as being proportional to the Cauchy probability distribution function  $\text{Cauchy}(y, \mathcal{A}(\mathcal{D}(\hat{z}_l^0)), \kappa)$ . Using the Cauchy probability distribution function as a likelihood function for particle filters has improved performance in various applications (Khine, Kuptamete, and Aunsri 2023; Jiang et al. 2023). This distribution, with a selection of  $\kappa = 1$ , would be proportionate to the inverse of the L2 distance between the measurement  $y$  and the output of the forward model  $\mathcal{A}(\mathcal{D}(\hat{z}_l^0))$ , with an added constant of 1, which ensures the function remains bounded. The details of this modeling and simplification will be shown in the supplementary materials. Thus,

$$p(y|\hat{z}_l^0) \propto \text{Cauchy}(y, \mathcal{A}(\mathcal{D}(\hat{z}_l^0)), 1) \\ \propto \frac{1}{\|y - \mathcal{A}(\mathcal{D}(\hat{z}_l^0))\|_2^2 + 1}. \quad (6)$$

**Prediction** Generating a new set of particles starts by drawing a new particle  $z_l^{t-1}$  from the proposal distribution. The proposal distribution function,  $q(z_l^{t-1}|z_l^t, y)$ , is unknown, but instead is approximated using the method of PSLD (Rout et al. 2023b) involving a gluing function,  $\text{gluing}(\cdot)$ . Thus, the proposal distribution function is approximated as

$$q(z_l^{t-1}|z_l^t, y) \approx z_l^{t-1} - \text{gluing}(\mathcal{D}(\hat{z}_l^0)), \quad (7)$$

where  $z_l^{t-1}$  is calculated via

$$z_l^{t-1} \leftarrow \frac{\sqrt{\alpha^t}(1 - \bar{\alpha}^{t-1})}{1 - \bar{\alpha}^t} z_l^t + \frac{\sqrt{\bar{\alpha}^{t-1}}\beta^t}{1 - \bar{\alpha}^t} \hat{z}_l^0 + \tilde{\sigma}^t \epsilon \\ z_l^{t-1} \leftarrow z_l^{t-1} - \eta_t \nabla_{z_l^t} \|y - \mathcal{A}(\mathcal{D}(\hat{z}_l^0))\|_2^2 \quad (8)$$

as specified and explained in PSLD. Note that  $\epsilon \sim \mathcal{N}(0, I)$ , and  $\tilde{\sigma}^t$  is provided by the trained diffusion model. In equation (8), intermediate estimates  $\hat{z}_l^0$  are directly produced using the score function  $s_\theta$  of the diffusion model, through

$$\hat{z}_l^0 \leftarrow \frac{1}{\sqrt{\alpha^t}} (z_l^t + (1 - \bar{\alpha}^t) s_\theta(z_l^t, t)). \quad (9)$$

Producing intermediate estimates,  $\hat{z}_l^0$ , is the main step taken by the reverse SDE. In Algorithm 1, Equations (7), (8), and (9) are encapsulated by  $\text{PSLD}(\cdot)$  in line 7, for brevity.

---

#### Algorithm 1: Proposed PFLD method

---

**Input:**  $T, y, \mathcal{D}, \mathcal{A}, s_\theta, N, N_{th}, \text{PSLD}(\cdot), R$

**Output:**  $\mathcal{D}(\hat{z}^0)$

```

1: // Generating N samples from p_T
2:  $\mathcal{Z} \leftarrow \{z_l^T \sim \mathcal{N}(0, I) | l \in [1, \dots, N]\}$ 
3:  $\mathcal{W} \leftarrow \emptyset$ 
4: // Reverse SDE
5: for  $t \leftarrow T - 1$  to 0 do
6:   for  $l \leftarrow 1$  to  $N$  do
7:      $\hat{z}_l^0, z_l^{t-1} \leftarrow \text{PSLD}(y, \mathcal{D}, \mathcal{A}, s_\theta)$ 
8:      $w_l^{t-1} \leftarrow \frac{w_l^t}{\|y - \mathcal{A}(\mathcal{D}(\hat{z}_l^0))\|_2^2 + 1}$ 
9:      $\mathcal{W} \leftarrow \mathcal{W} \cup \{w_l^{t-1}\}$ 
10:   end for
11: // Normalizing the weights
12:  $\mathcal{W} \leftarrow \left\{ w \left( \sum_{l=1}^N w_l \right)^{-1} \mid w \in \mathcal{W} \right\}$ 
13: // Resampling
14:  $N_d \leftarrow$  Equation (5)
15: if  $N_d \leq N_{th}$  then
16:   Resample particles with replacement based on their weights  $\mathcal{W}$ .
17: end if
18: // Particle pruning
19: if  $t \bmod R = 0$  and  $N > 1$  then
20:   Remove half of the particles with the smallest  $w$ 
21:    $N \leftarrow \lfloor \frac{N}{2} \rfloor$ 
22: end if
23: end for
24: return  $\mathcal{D}(\hat{z}^0)$ 

```

---

**Updating the weights** Our goal is for those particles likely to be near the solution at the end of reverse diffusion to remain and guide the overall particle population. Thus, particles should be weighted based on the closeness of  $\hat{z}_l^0$ , rather than the current particle state,  $z_l^t$ . Given the the measurement  $y$ , we propose updating weights according to

$$w_l^{t-1} \leftarrow \frac{w_l^t}{\|y - \mathcal{A}(\mathcal{D}(\hat{z}_l^0))\|_2^2 + 1}. \quad (10)$$

In our proposed weighting function, we incorporate only the likelihood PDF  $p(y|\hat{z}_l^0)$ , made explicit in Equation (13), and we did not consider  $q(z_l^t|z_l^{t-1}, m^t)$  and  $p(m^t|z_l^t)$  as is suggested in many particle filtering applications (Doucet, Godsill, and Andrieu 2000). Weights are normalized such that they sum to 1. Steps for updating the weights are shown in lines 8, 9, and 12 of Algorithm 1. More details related to this section and, specifically, the method of updating weights are given in the supplementary materials.

**Resampling and particle pruning** Resampling is performed any time that the degeneracy metric,  $N_d$ , calculated via equation (5), falls below the resampling threshold,  $N_{th}$ .

The last step in our PFLD algorithm is to reduce the particle population size in order to increase the method’s speed (making PFLD advantageous vs. simply running an existing LDM-based estimator multiple times to achieve a similar re-

Table 1: Results for tasks of Super-resolution ( $\times 8$ ) and Gaussian Deblurring evaluated on FFHQ-1K ( $512 \times 512$ ) and ImageNet-1K ( $512 \times 512$ ) datasets. We compute results only for our method (first two rows). All other results are drawn from (Rout et al. 2024). Best results are **bolded** and second best are underlined. In all cases, Stable Diffusion v-1.4 and the same measurement operators as in STSL (Rout et al. 2024) are used. As shown, our PFLD-10 model outperforms PSLD (identical to PFLD-1, our framework with a *single* particle) as a result of its ability to search solution space.

Method	FFHQ-1K ( $512 \times 512$ )						ImageNet-1K ( $512 \times 512$ )					
	SR ( $\times 8$ )			Gaussian Deblur			SR ( $\times 8$ )			Gaussian Deblur		
	LPIPS ( $\downarrow$ )	PSNR ( $\uparrow$ )	SSIM ( $\uparrow$ )	LPIPS ( $\downarrow$ )	PSNR ( $\uparrow$ )	SSIM ( $\uparrow$ )	LPIPS ( $\downarrow$ )	PSNR ( $\uparrow$ )	SSIM ( $\uparrow$ )	LPIPS ( $\downarrow$ )	PSNR ( $\uparrow$ )	SSIM ( $\uparrow$ )
PFLD-10 (Ours)	0.384	31.52	89.52	<u>0.361</u>	<b>32.59</b>	93.91	0.467	<u>30.48</u>	81.40	<u>0.385</u>	<b>31.35</b>	<u>88.77</u>
PFLD-1 (PSLD)	0.405	31.31	88.56	0.364	<u>32.54</u>	93.90	0.490	30.23	79.71	0.388	<u>31.30</u>	88.22
PSLD (Rout et al. 2023b)	0.402	31.39	88.89	0.371	32.26	92.63	0.484	30.23	80.72	0.387	31.20	88.65
STSL (Rout et al. 2024)	<b>0.335</b>	31.77	91.32	<b>0.308</b>	32.30	<b>94.04</b>	<b>0.392</b>	<b>30.64</b>	<b>84.86</b>	<b>0.349</b>	31.03	<b>90.21</b>
P2L	0.381	31.36	89.14	0.382	31.63	90.89	<u>0.441</u>	30.38	<u>84.27</u>	0.402	30.70	87.92
GML-DPS	0.368	<u>32.34</u>	<u>92.69</u>	0.370	32.33	92.65	0.482	30.35	81.01	0.387	31.19	88.60
LDPS	<u>0.354</u>	<b>32.54</b>	<b>93.46</b>	0.385	32.18	92.34	0.480	30.25	80.87	0.402	31.14	88.19
DPS (Chung et al. 2022)	0.538	29.15	72.92	0.694	28.14	56.15	0.522	29.18	70.72	0.647	28.11	55.40
DiffPIR	0.791	28.12	42.66	0.614	29.06	73.51	0.740	28.17	42.80	0.612	28.93	68.67

sult). Since the changes in particle state become smaller and smaller as  $t \rightarrow 0$ , (Ho, Jain, and Abbeel 2020), it is most advantageous to maintain a high population early in the reverse diffusion process, quickly and broadly exploring the solution space, then, pruning the population down to include only the best particles, which are allowed to continue until  $t = 0$ . The particle weights,  $w_t^i$ , act as the measure of particle fitness for the purpose of pruning, with larger weights being favoured.

Particle pruning is performed every  $R$  steps of the reverse diffusion process and at  $3R$  steps, only the single particle with largest weight will continue the reverse diffusion process. A naïve implementation simply reduces the population size by a factor of 2 at each occurrence of pruning. The parameter  $R$  determines the particle pruning schedule and, in this simple case, acts analogously to the *half-life* of exponentially decaying quantities, utilized across science (Rutherford 1900).

Though PSLD is used as a foundation upon which to evaluate the framework proposed in this paper, in principle, *any* diffusion-based method could be used. Furthermore, more sophisticated particle filtering methods could (and perhaps should) be used, incorporating resampling and more representative measures to be used as particle weights.

## 4 Results and Evaluation

The experimental setup by which our method is evaluated is first discussed, followed by the actual experimental results. The experiments performed are primarily motivated those of PSLD and STSL such that direct comparisons can be made. Each experiment is conducted on an NVIDIA A100 GPU. We choose the Stable Diffusion v-1.4 model (Rombach et al. 2022) and the same measurement operators as in STSL (Rout et al. 2024).

### 4.1 Experimental Setup

**Datasets** Two datasets are used for our evaluation: FFHQ-1K  $512 \times 512$  (Karras, Laine, and Aila 2019) and ImageNet-1K (Deng et al. 2009). From FFHQ-1K, the exact same selection method of 1000 images are used as in STSL (Rout et al. 2023a). Because the diffusion model, Stable Diffusion

v-1.4 (Rombach et al. 2022), was trained on FFHQ, images from this dataset are considered in-distribution, whereas for ImageNet-1K, the images are out-of-distribution.

**Baseline methods** PSLD serves as the primary baseline, given that it is used as the foundation upon which the framework of our method, PFLD, is demonstrated in this paper. DPS serves as a gold-standard baseline for pixel-space methods, and STSL (Rout et al. 2023a) (“Beyond First-Order Tweedie”), a latent-space method, is the current state-of-the-art on many tasks and can be considered an improved version of PSLD; however, its implementation code is not yet available.

**Inverse Tasks** As was introduced in Preliminaries, many inverse tasks within the space of image processing exist; however, for the evaluation of our method in this paper, we focus on eight-fold super-resolution, abbreviated SR ( $\times 8$ ), Gaussian deblurring and inpainting. For super-resolution and Gaussian deblurring, we follow the same setup of STSL (Rout et al. 2023a), whereas for inpainting, we consider a square mask with size of  $192 \times 192$  at the center of each image. For all tasks, the noise level is set to  $\sigma_v = 0.01$ .

**Metrics** Standard metrics are used to evaluate the performance of our method: Learned Perceptual Image Patch Similarity (LPIPS) (Zhang et al. 2018), peak signal-to-noise ratio (PSNR) (Gonzalez 2009) and structural similarity index measure (SSIM) (Wang et al. 2004). PSNR measures the quality of image reconstruction and does not consider local relationships between pixels in the image, hence we also report SSIM, which is sensitive to the local structure. LPIPS leverages neural network activations (in this work we use VGGNet (Simonyan and Zisserman 2015) weights) to evaluate perceptual similarity between a ground truth and a reconstructed image. Because metrics do not fully capture the visual quality of images, we also provide some resultant images for qualitative visual inspection.

**PFLD hyper-parameters** For our proposed method, we use  $N = 10$  as it is shown a reasonable choice based on the Figure 4. The other parameter that we used here is the particle pruning schedule  $R$  for which we select a medium

rate ( $R = 20$ ) as shown in Table 3 to have a balance between running time and performance. The resampling threshold  $N_{th}$  is set to  $\frac{N}{2}$  as discussed in (Doucet et al. 2001).

## 4.2 Experimental Results

We report quantitative results for our method, PFLD, in Tables 1 and 2 and show qualitative samples in Figure 3. More qualitative examples can be found in the supplementary material.

For the super-resolution task we have observed qualitatively better performance from PFLD-10. For example, PFLD has generally performed better when reconstructing parts of human faces and text, being visually closer to the ground truth. For the inpainting task, PFLD-10 yielded fewer artefacts, and in general, better perceptual quality, in particular for images of human faces. For the Gaussian deblurring task, most outputs from PSLD and PFLD-10 were comparable in perceptual quality.

Table 1 summarizes SR ( $\times 8$ ) and Gaussian deblurring results for not only PFLD and PSLD, but also the reported results of several other baseline methods. Our method, PFLD, is primarily compared to the PSLD method. Note that PFLD with only *one* particle should perform the same as PSLD, barring the effects of random initialization. Indeed, Table 1 shows that PFLD-1 replicates reported PSLD results on both datasets for the tasks of super-resolution and Gaussian deblurring. PFLD-10 improves upon PFLD-1 (and PSLD) for all metrics. Improvements on Gaussian deblurring are small because of artifacts, visible in Figure 3, which are inherent to PSLD and therefore affect results from PFLD.

Table 2 shows the comparison between PFLD-10 and PSLD on the inpainting task on both datasets. PFLD-10 outperforms PSLD on FFHQ-1K ( $512 \times 512$ ) for all metrics, but has mixed results on the out-of-distribution dataset, ImageNet-1K ( $512 \times 512$ ). In particular, PFLD scores marginally lower on PSNR and SSIM for this dataset. Because the diffusion model was fine-tuned on the FFHQ-1K ( $512 \times 512$ ) dataset, the samples generated will follow a distribution similar to that of the FFHQ-1K ( $512 \times 512$ ) dataset. Thus, the performance on the FFHQ-1K ( $512 \times 512$ ) dataset is expected to be better than on ImageNet-1K ( $512 \times 512$ ).

Figure 5 shows the effect that varying the number of initial particles has on the running time of the PFLD algorithm, and makes a comparison to simply running PSLD an equivalent number of times. The concept largely motivating PFLD is the hypothesis that running PFLD with a given number of initial particles will achieve similar results as selecting the best result generated from running PSLD an equivalent number of times, but that PFLD will take far less time. Indeed, the runtime of PSLD when executed multiple times *far* exceeds that of PFLD, growing at a rate roughly  $16\times$  larger for the  $R = 20$  pruning schedule. Clearly, even for modest numbers, running PFLD is a far more efficient method of robustly generating solution estimates.

**Ablation Studies** To better understand several key attributes of our method, we perform two ablation studies.

In the first study, we determine the impact that the starting number of particles,  $N$ , has on the quality of resultant

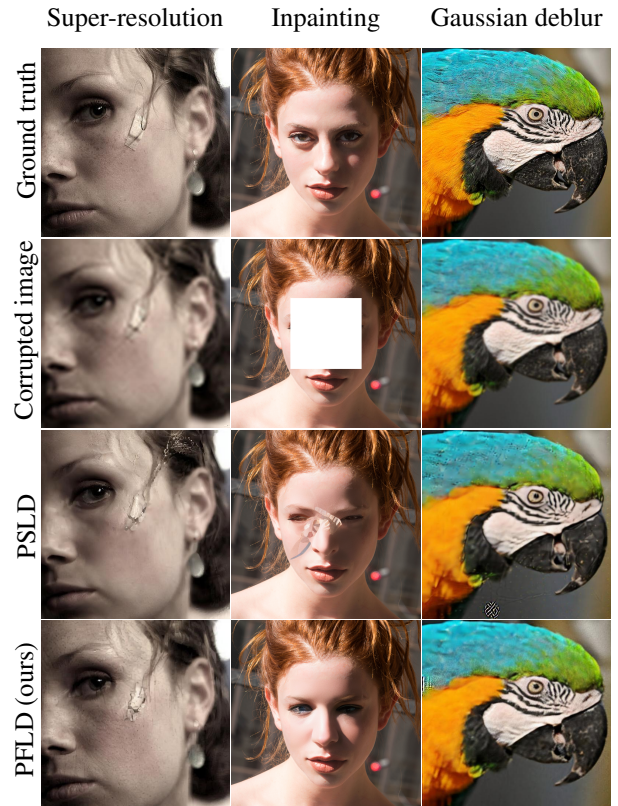


Figure 3: Qualitative results. For the super-resolution task, PFLD reconstructs the face with more detail (freckles, wrinkles), while PSLD struggles to accurately reconstruct the lock of hair falling onto the bandage. For the inpainting task PSLD struggled to accurately reconstruct the eyes and the bridge of the nose, while PFLD achieved a believable result. For the Gaussian deblurring task PFLD generated a slightly sharper image with fewer artifacts. The image in the first and third columns of this figure are from ImageNet-1K and the inpainting example is from FFHQ-1K ( $512 \times 512$ ).

Table 2: Results of running PFLD-10 and PSLD (PFLD-1) on the inpainting task on FFHQ-1K ( $512 \times 512$ ) and ImageNet-1K ( $512 \times 512$ ) datasets. Stable Diffusion v-1.4 is used for this result with a fixed mask of  $192 \times 192$  in the center of each image. Best results are **bolded**.

Method	FFHQ-1K ( $512 \times 512$ )			ImageNet-1K ( $512 \times 512$ )		
	LPIPS ( $\downarrow$ )	PSNR ( $\uparrow$ )	SSIM ( $\uparrow$ )	LPIPS ( $\downarrow$ )	PSNR ( $\uparrow$ )	SSIM ( $\uparrow$ )
PFLD-10 (Ours)	<b>0.0694</b>	<b>36.71</b>	<b>91.93</b>	<b>0.0979</b>	36.80	84.77
PFLD-1 (PSLD)	0.0707	36.70	91.65	0.0982	<b>36.81</b>	<b>84.78</b>

images, measured by both mean metrics and their standard deviation, to indicate the level of reliability or robustness. Only the first 10 images of FFHQ-1K ( $512 \times 512$ ) are used, and tasks of SR ( $\times 8$ ) and Gaussian deblurring are studied. Results for this study are shown in Figure 4. Observe that for both tasks, increasing the number of particles leads to

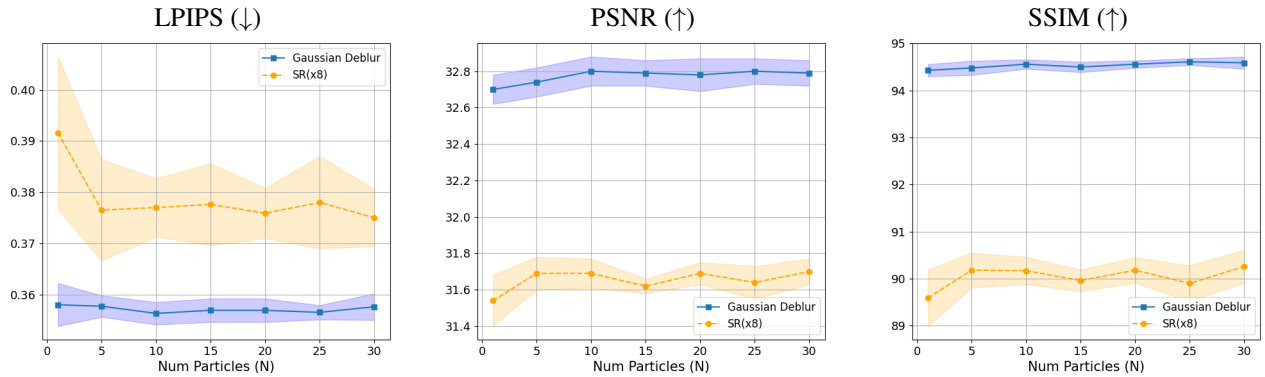


Figure 4: The effect of varying the number of particles 1, 5, 10, 15, 20, 25, 30 on different metrics on the first 10 images of FFHQ-1K ( $512 \times 512$ ) dataset on two tasks: Super Resolution ( $\times 8$ ) and Gaussian Deblurring. We repeated each experiment 10 times. The shaded regions show the standard deviation of each experiments, indicating the degree of variance in the results.

Table 3: Ablation study on the impact of having a more or less aggressive particle pruning schedule on PFLD, evaluated on the first 100 images of FFHQ-1K ( $512 \times 512$ ). We compare three schedules characterized by their rate of pruning: aggressive ( $R = 10$ ), medium ( $R = 20$ ), and gentle ( $R = 30$ ). Best results are **bolded**. More rapid pruning results in a decrease in runtime, whereas more gradual pruning offers a prolonged ability to search the latent space and better results.

Pruning Schedule ( $R$ )	SR ( $\times 8$ )			Gaussian Deblur		
	LPIPS (↓)	PSNR (↑)	SSIM (↑)	LPIPS (↓)	PSNR (↑)	SSIM (↑)
10	0.3797	31.56	87.54	0.3564	32.74	93.56
20	0.3765	31.62	87.75	0.3559	32.80	93.61
30	<b>0.3730</b>	<b>31.79</b>	<b>87.97</b>	<b>0.3514</b>	<b>32.85</b>	<b>94.45</b>

an upward trend for PSNR and SSIM, as well as a downward trend for LPIPS, while simultaneously reducing the variance. The results also indicate that the largest rate of improvement comes from adding modest numbers of particles to the single-particle base-case, for which performance metrics most rapidly improve and standard deviation shrinks.

The second ablation study explores the impacts of varying the aggressiveness of the particle pruning schedule and is analogous to an annealing schedule, popularized through its use in the simulated annealing (Van Laarhoven et al. 1987) technique for solving optimization problems. We compare three pruning schedules, parameterized by the number of time steps between pruning,  $R = 10, 20, 30$ . Performance (LPIPS, PSNR, SSIM) is shown for all three schedules in Table 3. More rapid pruning reduces computational cost, whereas gradual pruning allows for a more extensive search of the latent space and produces better results.

## 5 Conclusion

PFLD, a novel framework for solving inverse problems is presented here. The framework incorporates a particle filter on top of existing diffusion-based inverse-problem solvers, yielding improvements both to the average perfor-

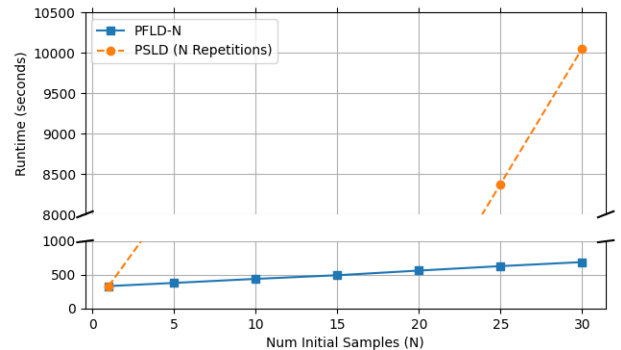


Figure 5: The effect of varying the number of initial particles on the running time of the PFLD algorithm. Results are shown for the SR ( $\times 8$ ) inverse problem for a single image from the FFHQ-1K  $512 \times 512$  dataset. Furthermore, a comparison to the time required to simply run PSLD an equivalent number of times is given, where it is clear that PFLD is far more efficient. As illustrated, having many initial particles and then pruning allows the proposed PFLD method to broadly explore the solution space while still being efficient. The runtime for repeated PSLD is linear with the number of repetitions,  $N$ .

mance and robustness. This was demonstrated on a state-of-the-art method, PSLD, using only a naïve particle filter. Improvements were made for tasks of super-resolution, Gaussian deblurring and inpainting on both the FFHQ-1K  $512 \times 512$  (Karras, Laine, and Aila 2019) and ImageNet-1K (Deng et al. 2009) datasets. Future work will explore the use of more sophisticated particle filtering schemes, specifically incorporating resampling and particle weights that more closely relate to the visual quality of end-results.

## References

Arulampalam, M. S.; Maskell, S.; Gordon, N.; and Clapp, T. 2002. A tutorial on particle filters for online nonlinear/non-

- Gaussian Bayesian tracking. *IEEE Transactions on signal processing*, 50(2): 174–188.
- Bansal, A.; Borgnia, E.; Chu, H.-M.; Li, J.; Kazemi, H.; Huang, F.; Goldblum, M.; Geiping, J.; and Goldstein, T. 2024. Cold diffusion: Inverting arbitrary image transforms without noise. *Advances in Neural Information Processing Systems*, 36.
- Bertero, M.; Boccacci, P.; and De Mol, C. 2021. *Introduction to inverse problems in imaging*. CRC press.
- Cao, H.; Tan, C.; Gao, Z.; Xu, Y.; Chen, G.; Heng, P.-A.; and Li, S. Z. 2024. A survey on generative diffusion models. *IEEE Transactions on Knowledge and Data Engineering*.
- Chung, H.; Kim, J.; Mccann, M. T.; Klasky, M. L.; and Ye, J. C. 2022. Diffusion posterior sampling for general noisy inverse problems. *arXiv preprint arXiv:2209.14687*.
- Chung, H.; Ye, J. C.; Milanfar, P.; and Delbracio, M. 2023. Prompt-tuning latent diffusion models for inverse problems. *arXiv preprint arXiv:2310.01110*.
- Compton, K.; Osborn, J. C.; and Mateas, M. 2013. Generative methods. In *The fourth procedural content generation in games workshop, pcg*, volume 1.
- Croitoru, F.-A.; Hondru, V.; Ionescu, R. T.; and Shah, M. 2023. Diffusion models in vision: A survey. *IEEE Transactions on Pattern Analysis and Machine Intelligence*, 45(9): 10850–10869.
- Daras, G.; Delbracio, M.; Talebi, H.; Dimakis, A.; and Milanfar, P. 2023. Soft Diffusion: Score Matching with General Corruptions. *Transactions on Machine Learning Research*.
- Deja, K.; Kuzina, A.; Trzcinski, T.; and Tomczak, J. 2022. On analyzing generative and denoising capabilities of diffusion-based deep generative models. *Advances in Neural Information Processing Systems*, 35: 26218–26229.
- Deng, J.; Dong, W.; Socher, R.; Li, L.-J.; Li, K.; and Fei-Fei, L. 2009. Imagenet: A large-scale hierarchical image database. In *2009 IEEE conference on computer vision and pattern recognition*, 248–255. Ieee.
- Dimakis, A. G. 2022. Deep generative models and inverse problems. *Mathematical Aspects of Deep Learning*, 400.
- Djuric, P. M.; Kotecha, J. H.; Zhang, J.; Huang, Y.; Ghirmai, T.; Bugallo, M. F.; and Míguez, J. 2003. Particle filtering. *IEEE signal processing magazine*, 20(5): 19–38.
- Doucet, A.; De Freitas, N.; Gordon, N. J.; et al. 2001. *Sequential Monte Carlo methods in practice*, volume 1. Springer.
- Doucet, A.; Godsill, S.; and Andrieu, C. 2000. On sequential Monte Carlo sampling methods for Bayesian filtering. *Statistics and computing*, 10: 197–208.
- Doucet, A.; Godsill, S. J.; and Andrieu, C. 1998. *On sequential simulation-based methods for Bayesian filtering*. Department of Engineering, University of Cambridge Cambridge, UK.
- Doucet, A.; Johansen, A. M.; et al. 2009. A tutorial on particle filtering and smoothing: Fifteen years later. *Handbook of nonlinear filtering*, 12(656-704): 3.
- Fieguth, P. 2010. *Statistical image processing and multidimensional modeling*. Springer Science & Business Media.
- Gonzalez, R. C. 2009. *Digital image processing*. Pearson education india.
- Gordon, N.; Ristic, B.; and Arulampalam, S. 2004. Beyond the kalman filter: Particle filters for tracking applications. *Artech House, London*, 830(5): 1–4.
- Graikos, A.; Malkin, N.; Jojic, N.; and Samaras, D. 2022. Diffusion models as plug-and-play priors. *Advances in Neural Information Processing Systems*, 35: 14715–14728.
- Harshvardhan, G.; Gourisaria, M. K.; Pandey, M.; and Rautaray, S. S. 2020. A comprehensive survey and analysis of generative models in machine learning. *Computer Science Review*, 38: 100285.
- Ho, J.; Jain, A.; and Abbeel, P. 2020. Denoising diffusion probabilistic models. *Advances in neural information processing systems*, 33: 6840–6851.
- Hu, J.; Song, B.; Xu, X.; Shen, L.; and Fessler, J. A. 2024. Learning Image Priors through Patch-based Diffusion Models for Solving Inverse Problems. *arXiv preprint arXiv:2406.02462*.
- Jiang, C.; Zhu, D.; Li, H.; Xu, X.; and Li, D. 2023. Improving the particle filter for data assimilation in hydraulic modeling by using a Cauchy likelihood function. *Journal of Hydrology*, 617: 129050.
- Karras, T.; Laine, S.; and Aila, T. 2019. A style-based generator architecture for generative adversarial networks. In *Proceedings of the IEEE/CVF conference on computer vision and pattern recognition*, 4401–4410.
- Khine, M. H. H.; Kuptamettee, C.; and Aunsri, N. 2023. Improving Reliability of State Estimation by Particle Filter with Cauchy Likelihood Function. In *2023 7th International Conference on Information Technology (InCIT)*, 556–561. IEEE.
- Lunz, S.; Öktem, O.; and Schönlieb, C.-B. 2018. Adversarial regularizers in inverse problems. *Advances in neural information processing systems*, 31.
- Rombach, R.; Blattmann, A.; Lorenz, D.; Esser, P.; and Ommer, B. 2022. High-resolution image synthesis with latent diffusion models. In *Proceedings of the IEEE/CVF conference on computer vision and pattern recognition*, 10684–10695.
- Rout, L.; Chen, Y.; Kumar, A.; Caramanis, C.; Shakkottai, S.; and Chu, W.-S. 2023a. Beyond First-Order Tweedie: Solving Inverse Problems using Latent Diffusion. *arXiv preprint arXiv:2312.00852*.
- Rout, L.; Chen, Y.; Kumar, A.; Caramanis, C.; Shakkottai, S.; and Chu, W.-S. 2024. Beyond first-order tweedie: Solving inverse problems using latent diffusion. In *Proceedings of the IEEE/CVF Conference on Computer Vision and Pattern Recognition*, 9472–9481.
- Rout, L.; Raoof, N.; Daras, G.; Caramanis, C.; Dimakis, A. G.; and Shakkottai, S. 2023b. Solving linear inverse problems provably via posterior sampling with latent diffusion models. *arXiv preprint arXiv:2307.00619*.
- Rutherford, E. 1900. I. A radio-active substance emitted from thorium compounds. *The London, Edinburgh, and Dublin Philosophical Magazine and Journal of Science*, 49(296): 1–14.



Salmond, D. J. 1990. Mixture reduction algorithms for target tracking in clutter. In *Signal and Data Processing of Small Targets 1990*, volume 1305, 434. SPIE.

Shah, V.; and Hegde, C. 2018. Solving linear inverse problems using gan priors: An algorithm with provable guarantees. In *2018 IEEE international conference on acoustics, speech and signal processing (ICASSP)*, 4609–4613. IEEE.

Simonyan, K.; and Zisserman, A. 2015. Very Deep Convolutional Networks for Large-Scale Image Recognition. arXiv:1409.1556.

Sohl-Dickstein, J.; Weiss, E.; Maheswaranathan, N.; and Ganguli, S. 2015. Deep unsupervised learning using nonequilibrium thermodynamics. In *International conference on machine learning*, 2256–2265. PMLR.

Song, Y.; and Ermon, S. 2020. Improved techniques for training score-based generative models. *Advances in neural information processing systems*, 33: 12438–12448.

Song, Y.; Sohl-Dickstein, J.; Kingma, D. P.; Kumar, A.; Ermon, S.; and Poole, B. 2020. Score-based generative modeling through stochastic differential equations. *arXiv preprint arXiv:2011.13456*.

Tewari, A.; Yin, T.; Cazenavette, G.; Rezhikov, S.; Tenenbaum, J.; Durand, F.; Freeman, B.; and Sitzmann, V. 2023. Diffusion with forward models: Solving stochastic inverse problems without direct supervision. *Advances in Neural Information Processing Systems*, 36: 12349–12362.

Van Laarhoven, P. J.; Aarts, E. H.; van Laarhoven, P. J.; and Aarts, E. H. 1987. *Simulated annealing*. Springer.

Wang, Z.; Bovik, A. C.; Sheikh, H. R.; and Simoncelli, E. P. 2004. Image quality assessment: from error visibility to structural similarity. *IEEE transactions on image processing*, 13(4): 600–612.

Welch, G.; Bishop, G.; et al. 1995. An introduction to the Kalman filter.

Zhang, R.; Isola, P.; Efros, A. A.; Shechtman, E.; and Wang, O. 2018. The unreasonable effectiveness of deep features as a perceptual metric. In *Proceedings of the IEEE conference on computer vision and pattern recognition*, 586–595.

## 6 Supplementary Materials

This section contains additional findings and specific information that were not included in the main part of the paper due to space constraints. Specifically, we provide in-depth theoretical analysis and detailed implementation information, as well as further qualitative analysis.

### 6.1 PSLD Results

Figure 6 shows an extension of Figure 2, showing different results of PSLD (Rout et al. 2023b) for different initializations of the PSLD algorithm, which is the main problem of diffusion-based solvers and the main motivation of the proposed Particle-Filtering-based Latent Diffusion (PFLD) methods.

### 6.2 Method

In PFLD, the likelihood PDF  $p(y|\hat{z}_l^0)$  is modeled as being proportional to the Cauchy probability distribution function Cauchy  $(y, \mathcal{A}(\mathcal{D}(\hat{z}_l^0)), \kappa)$ . The PDF of Cauchy distributing is defined as:

$$\text{Cauchy}(x; x_0, \kappa) = \frac{1}{\pi\kappa \left[1 + \left(\frac{x-x_0}{\kappa}\right)^2\right]} \quad (11)$$

By considering  $\kappa = 1$  Cauchy PDF is define as:

$$\text{Cauchy}(y; \mathcal{A}(\mathcal{D}(\hat{z}_l^0)), 1) = \frac{1}{\pi \left[1 + (y - \mathcal{A}(\mathcal{D}(\hat{z}_l^0)))^2\right]} \quad (12)$$

This distribution, with a selection of  $\kappa = 1$ , would be proportionate to the inverse of the L2 distance between the measurement  $y$  and the output of the forward model  $\mathcal{A}(\mathcal{D}(\hat{z}_l^0))$ , with an added constant of 1.

$$\begin{aligned} p(y|\hat{z}_l^0) &\propto \text{Cauchy}(y, \mathcal{A}(\mathcal{D}(\hat{z}_l^0)), 1) \\ &\propto \frac{1}{\|y - \mathcal{A}(\mathcal{D}(\hat{z}_l^0))\|_2^2 + 1}. \end{aligned} \quad (13)$$

**Updating the weights** From Equation (4), by replacing  $m^t$  by  $y$  and considering the current time index  $t - 1$ , and the previous time index  $t$  as we do a reverse SDE, we have:

$$w_l^{t-1} \propto w_l^t \frac{p(y|z_l^{t-1}) p(z_l^{t-1}|z_l^t)}{q(z_l^{t-1}|z_l^t, y)}. \quad (14)$$

Based on optimal important sampling which is explained in (Doucet, Godsill, and Andrieu 1998), we could consider  $q(z_l^{t-1}|z_l^t, y) \propto p(z_l^{t-1}|z_l^t)$ . Therefore, we can define updating the weights function as follows:

$$w_l^{t-1} \propto w_l^t p(y|\hat{z}_l^0), \quad (15)$$

and by plugging in the Equation (13) into Equation (15), updating the weights would be defined as:

$$w_l^{t-1} \leftarrow \frac{w_l^t}{\|y - \mathcal{A}(\mathcal{D}(\hat{z}_l^0))\|_2^2 + 1}. \quad (16)$$

as it defined in the Equation (16).

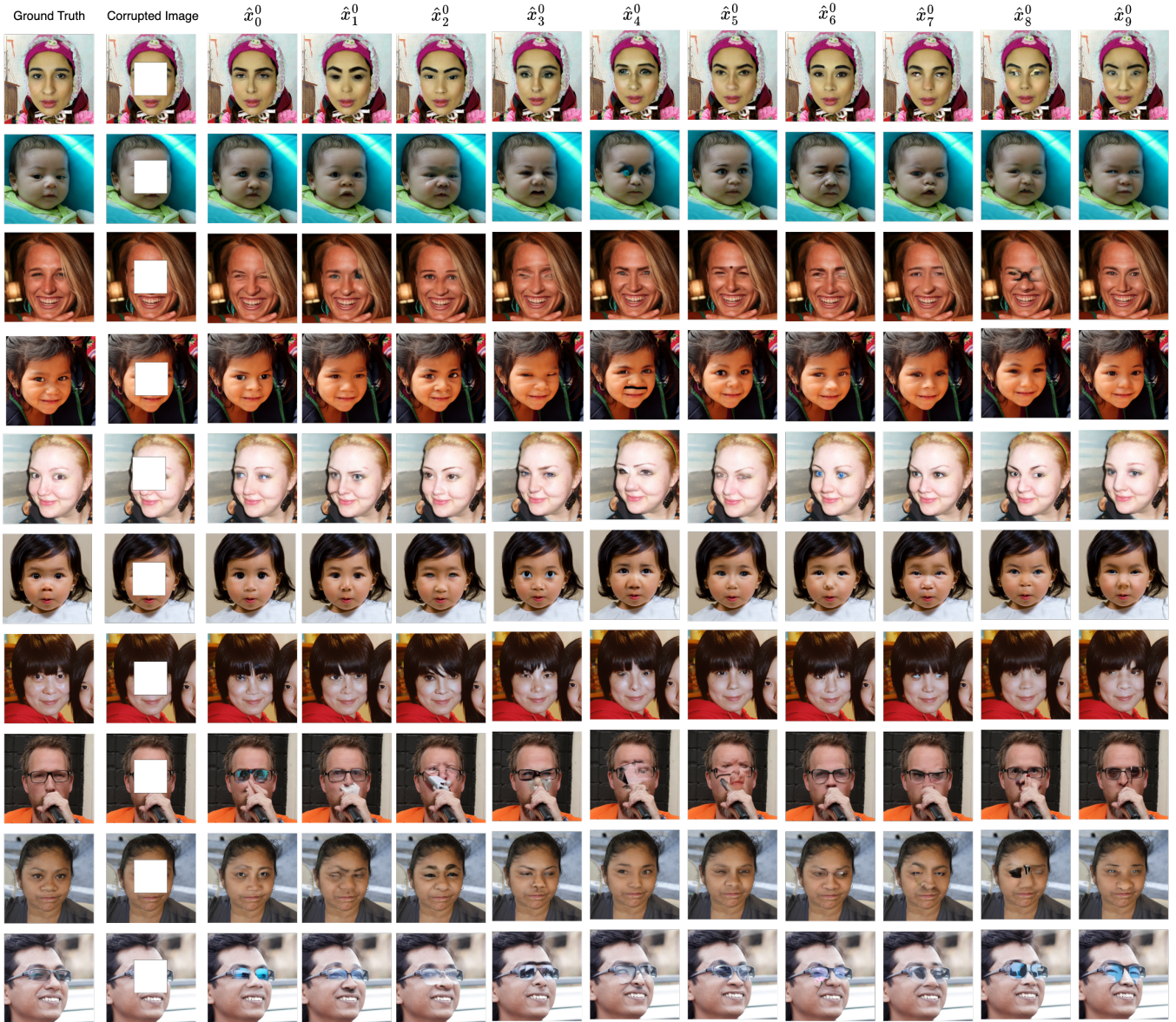


Figure 6: Ten different runs of PSLD (Rout et al. 2023b) were performed, each with a unique initialization and random seed, resulting in various outputs  $\hat{x}_i^0$ . The corrupted image used for inpainting had a mask measuring  $192 \times 192$  pixels, positioned in the center of the ground truth images. Images used in this figure are from the FFHQ dataset (Karras, Laine, and Aila 2019). The existing diffusion-based inverse problem solvers, such as PSLD, can yield diverse outcomes when initialized differently.

**PFLD algorithm** Algorithm 2 illustrates the PFLD method in depth when applied to PSLD, while Algorithm 1 was an abstract version of Algorithm 2. Lines 7,  $\dots$ , 12 of Algorithm 2 provide further information about PSLD( $\cdot$ ) which is mentioned in Section 3. Resampling and its interaction with particle pruning are also defined.

### 6.3 Results and Evaluation

**Quantitative results** Standard implementations of LPIPS, PSNR and SSIM metrics in *torchmetrics* package were used for calculating the quantitative results.

**Qualitative results** Figures 7, Figure 8, and Figure 9 demonstrate the higher performance of PFLD compared to PSLD in the super-resolution task. In this case, the same configuration, SR( $\times 8$ ), is employed for super-resolution. PFLD can enhance the performance of the base model PSLD in the inpainting task, provided that at least one of the 10 particles has a better reconstruction quality and there is a strong connection between the measurement  $y$  and the area beneath the mask. In Figure 9, this circumstance occurred. However, in Figure 8, the performance of PFLD and PSLD is nearly the same. The essential feature of PFLD in Gaussian deblur

---

**Algorithm 2: Proposed PFLD method**

---

**Input:**  $T, y, \mathcal{D}, \mathcal{A}, s_\theta, \gamma, N, N_{th}, \mathcal{A}x^*, R$ **Output:**  $\mathcal{D}(\hat{z}^0)$ 

```
1: // Generating  $N$  samples from  $p_T$ 
2:  $\mathcal{Z} \leftarrow \{z_l^T \sim \mathcal{N}(0, I) \mid l \in [1, \dots, N]\}$ 
3:  $\mathcal{W} \leftarrow \emptyset$ 
4: // Reverse SDE
5: for  $t \leftarrow T - 1$  to 0 do
6:   for  $l \leftarrow 1$  to  $N$  do
7:      $\hat{s} \leftarrow s_\theta(z_l^t, t)$ 
8:      $\hat{z}_l^0 \leftarrow \frac{1}{\sqrt{\bar{\alpha}^t}}(z_l^t + (1 - \bar{\alpha}^t)\hat{s})$ 
9:      $\epsilon \sim \mathcal{N}(0, I)$ 
10:     $z_l^{t-1} \leftarrow \frac{\sqrt{\bar{\alpha}^t(1-\bar{\alpha}^{t-1})}}{1-\bar{\alpha}^t}z_l^t + \frac{\sqrt{\bar{\alpha}^{t-1}\beta^t}}{1-\bar{\alpha}^t}\hat{z}_l^0 + \tilde{\sigma}^t\epsilon$ 
11:     $z_l''^{t-1} \leftarrow z_l^{t-1} - \eta_t \nabla_{z_l^t} \|y - \mathcal{A}(\mathcal{D}(\hat{z}_l^0))\|_2^2$ 
12:     $z_l^{t-1} \leftarrow z_l''^{t-1} - \gamma_i \nabla_{z_l^t} \|\hat{z}_l^0 - \mathcal{E}(\mathcal{A}^T \mathcal{A}x^* + (I - \mathcal{A}^T \mathcal{A})\mathcal{D}(\hat{z}_l^0))\|_2^2$ 
13:     $w_l^{t-1} \leftarrow \frac{w_l^t}{\|y - \mathcal{A}(\mathcal{D}(\hat{z}_l^0))\|_2^2 + 1}$ 
14:     $\mathcal{W} \leftarrow \mathcal{W} \cup \{w_l^{t-1}\}$ 
15:   end for
16:   // Normalizing the weights
17:    $\mathcal{W} \leftarrow \left\{ w \left( \sum_{l=1}^N w_l \right)^{-1} \mid w, w_l \in \mathcal{W} \right\}$ 
18:   // Resampling
19:    $N_d \leftarrow \frac{1}{\sum_{l=1}^N (w_l^t)^2}$ 
20:   if  $N_d \leq N_{th}$  then
21:     for  $l \leftarrow 1$  to  $N$  do
22:       draw  $j \sim \{1, \dots, N\}$  with prob.  $\propto w_l \in \mathcal{W}$ 
23:        $z_l^t \leftarrow z_j^{t-1}$ 
24:        $w_l \leftarrow w_j$ 
25:     end for
26:   end if
27:   // Particle pruning
28:   if  $t \bmod R = 0$  and  $N > 1$  then
29:     remove half of the particles with the smallest  $w$  from the set of particles and weights
30:      $N \leftarrow \lfloor \frac{N}{2} \rfloor$ 
31:   end if
32:   if  $N_d \leq N_{th}$  then
33:      $\mathcal{W} \leftarrow \{w \leftarrow \frac{1}{N} \mid w \in \mathcal{W}\}$ 
34:   end if
35: end for
36: return  $\mathcal{D}(\hat{z}^0)$ 
```

---

is its ability to enhance sharpness and effectively handle artifacts of PSLD. As an illustration, PFLD demonstrates superior performance compared to PSLD on Gaussian deblur task in Figure 7.

Figure 10 depicts an instance when PFLD fails to perform well on the super-resolution challenge. As previously stated, PFLD can achieve superior performance when at least one particle surpasses PSLD's initial point. Figure 10 shows that PFLD achieves similar performance to PSLD in inpainting and Gaussian deblur tasks.

Figures 7, Figure 8, and Figure 9 present a comparison of the performance of PFLD and PSLD for SR( $\times 8$ ) and Gaussian deblur tasks on the ImageNet-1K dataset. This compar-

ison is done using different shapes and textures in the images of the ImageNet-1K dataset instead of faces in FFHQ, as it allows for a clearer demonstration of these two tasks. Given that the primary numerical findings of the research are based on the FFHQ-1K  $512 \times 512$  dataset as well, Figures 11 and 12 illustrate the outcomes of PFLD and PSLD on the FFHQ-1K dataset. In terms of enhanced clarity and reduced artifacts in the resulting reconstructed image, the PFLD method outperforms the other method illustrated in these two figures.

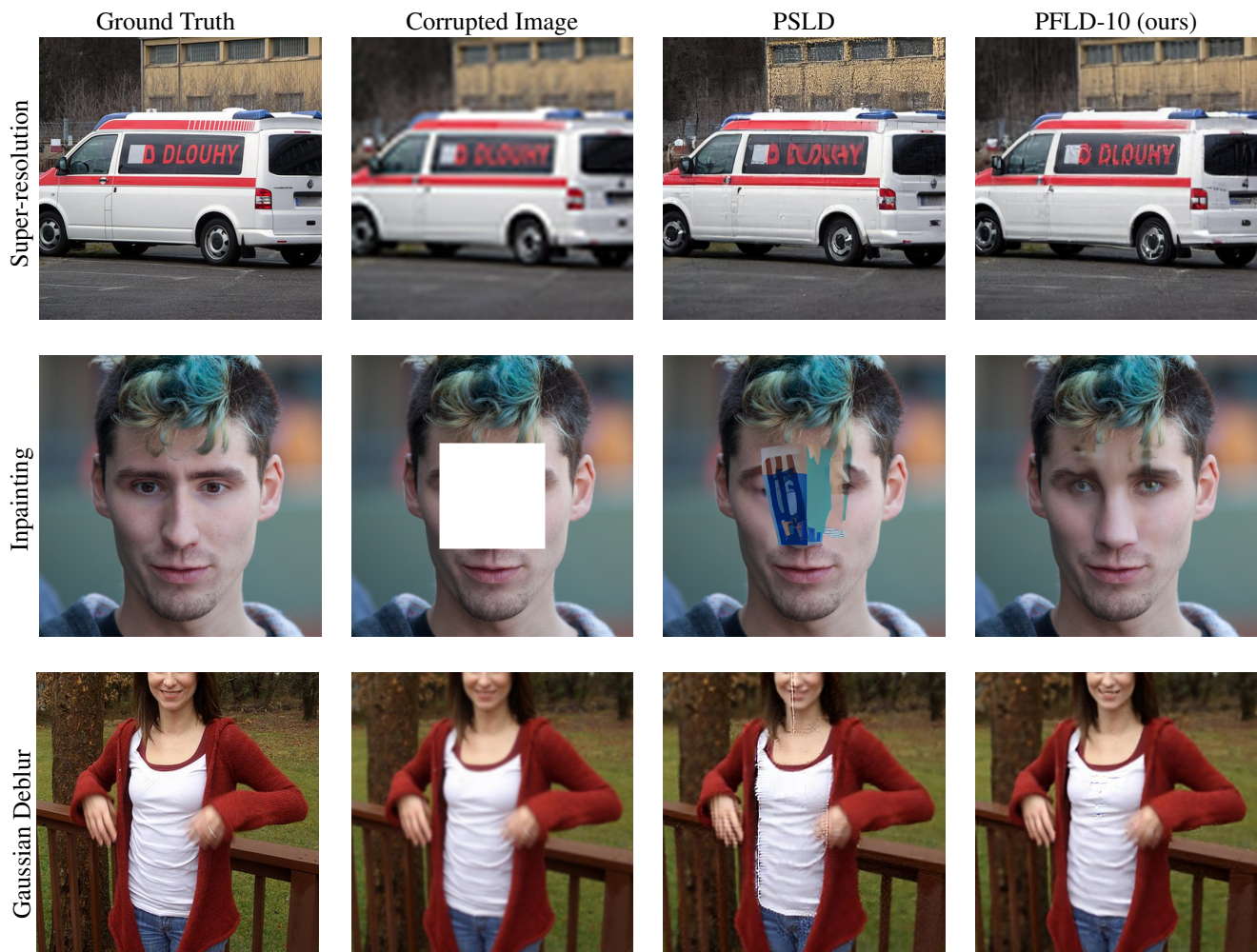


Figure 7: In the super-resolution task, PFLD performed a better reconstruction of the printed text on the ambulance, whereas PSLD struggled to do so. PSLD struggled to recreate the face for the inpainting task, whereas PFLD produced an acceptable outcome. During the Gaussian Deblur task, PFLD produced a slightly sharper image with fewer artifacts. The first and third rows of this figure show images from ImageNet-1K, while the inpainting example comes from FFHQ-1K ( $512 \times 512$ ).

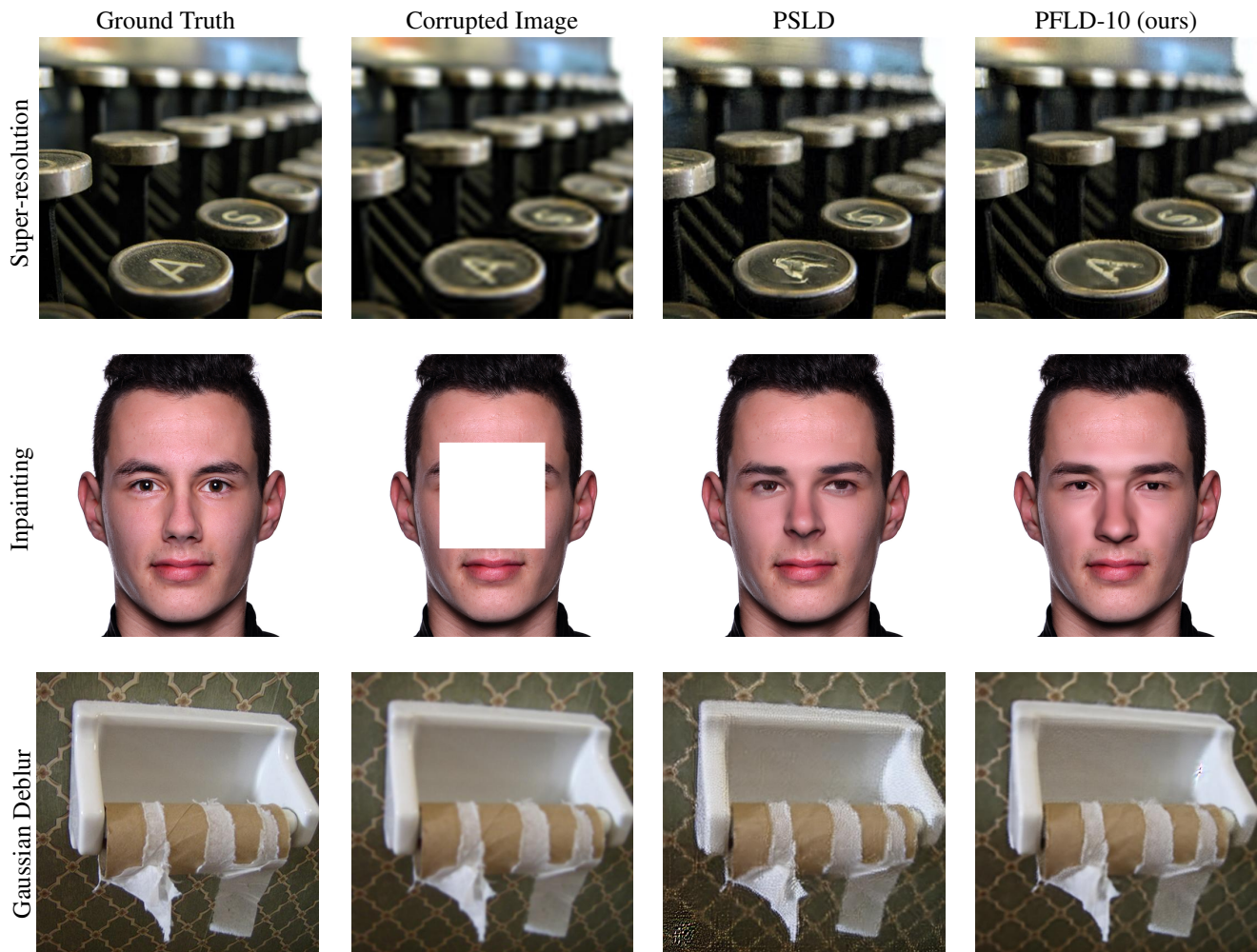


Figure 8: In the super-resolution task, PFLD reconstructed "A" and "S" better than PSLD; however, its performance in inpainting and Gaussian deblur is comparable to PSLD. The first and third rows of this figure show images from ImageNet-1K images are used for super resolution and Gaussian deblur and for inpainting FFHQ-1K (512 × 512) is used.

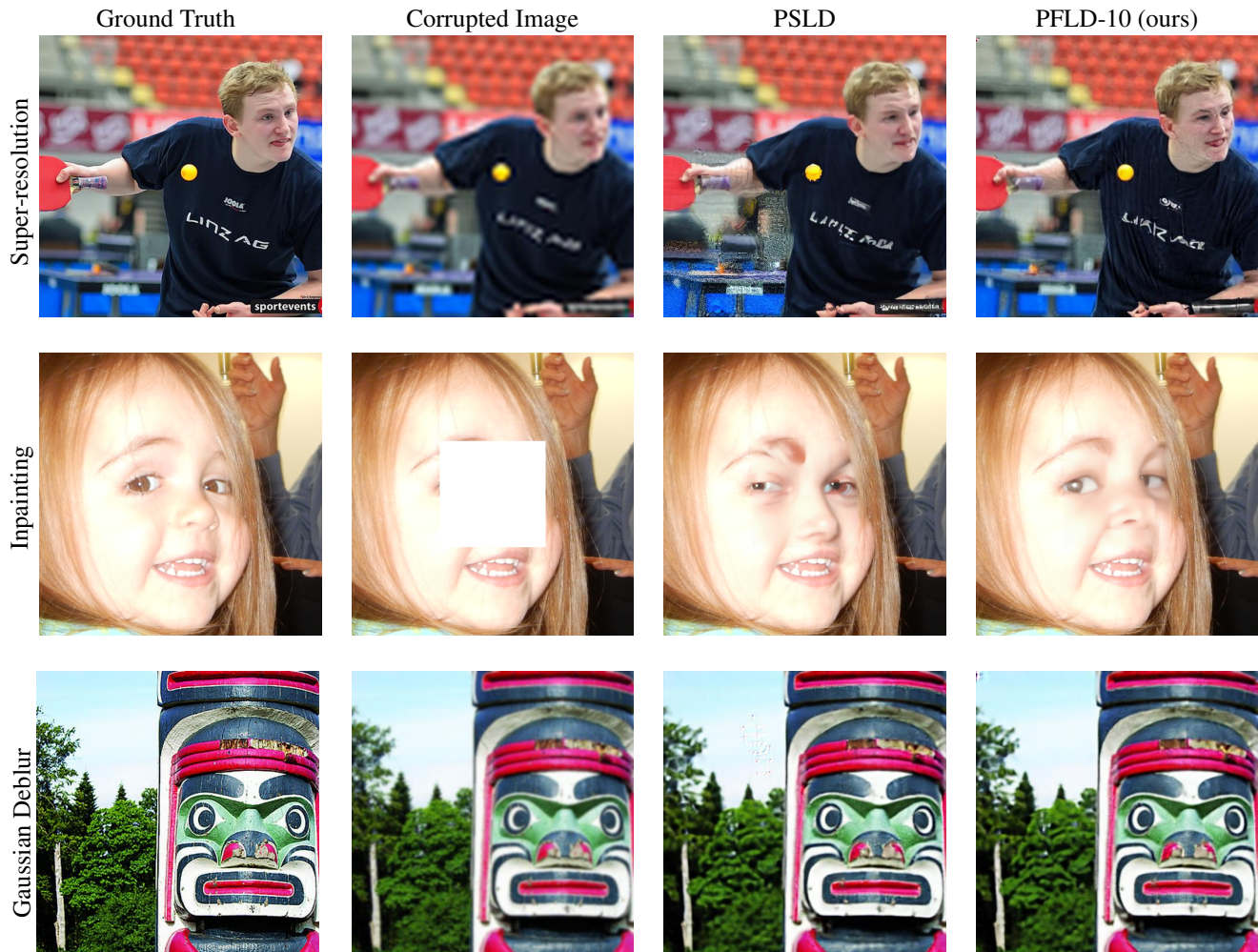


Figure 9: PFLD demonstrated superior performance in reconstructing the player’s face in the super-resolution task, but PS LD encountered difficulties in achieving the same level of reconstruction for Inpainting. PFLD also was able to generate a satisfactory result since it had access to sufficient information in the  $y$  variable and had learned stable diffusion patterns from the FFHQ dataset. For the Gaussian deblur task, the PFLD algorithm achieved comparable image quality to a PS LD image while having fewer artifacts. The photos displayed in the first and third rows of this figure are sourced from ImageNet-1K. The inpainting sample, on the other hand, is taken from FFHQ-1K  $512 \times 512$ .



Figure 10: Regarding the super-resolution task, PFLD showed inferior performance compared to PSLD. The fact that none of the ten initializations outperformed a single initialization for PSLD could potentially explain this. Inpainting and Gaussian Deblur offer similar outcomes as PSLD. Here again, first and third rows of this figure show images from ImageNet-1K, while the inpainting example comes from FFHQ-1K ( $512 \times 512$ ).



Figure 11: Qualitative results for the super-resolution task on the FFHQ-1K ( $512 \times 512$ ) dataset. For the first sample, PFLD-10 suffers from fewer artifacts than PSLD. For the second sample, PFLD-10 creates a slightly sharper output than PSLD. For the third sample, PSLD leaves a considerable amount of noise in the hair and face region; PFLD-10 output is visually smoother.



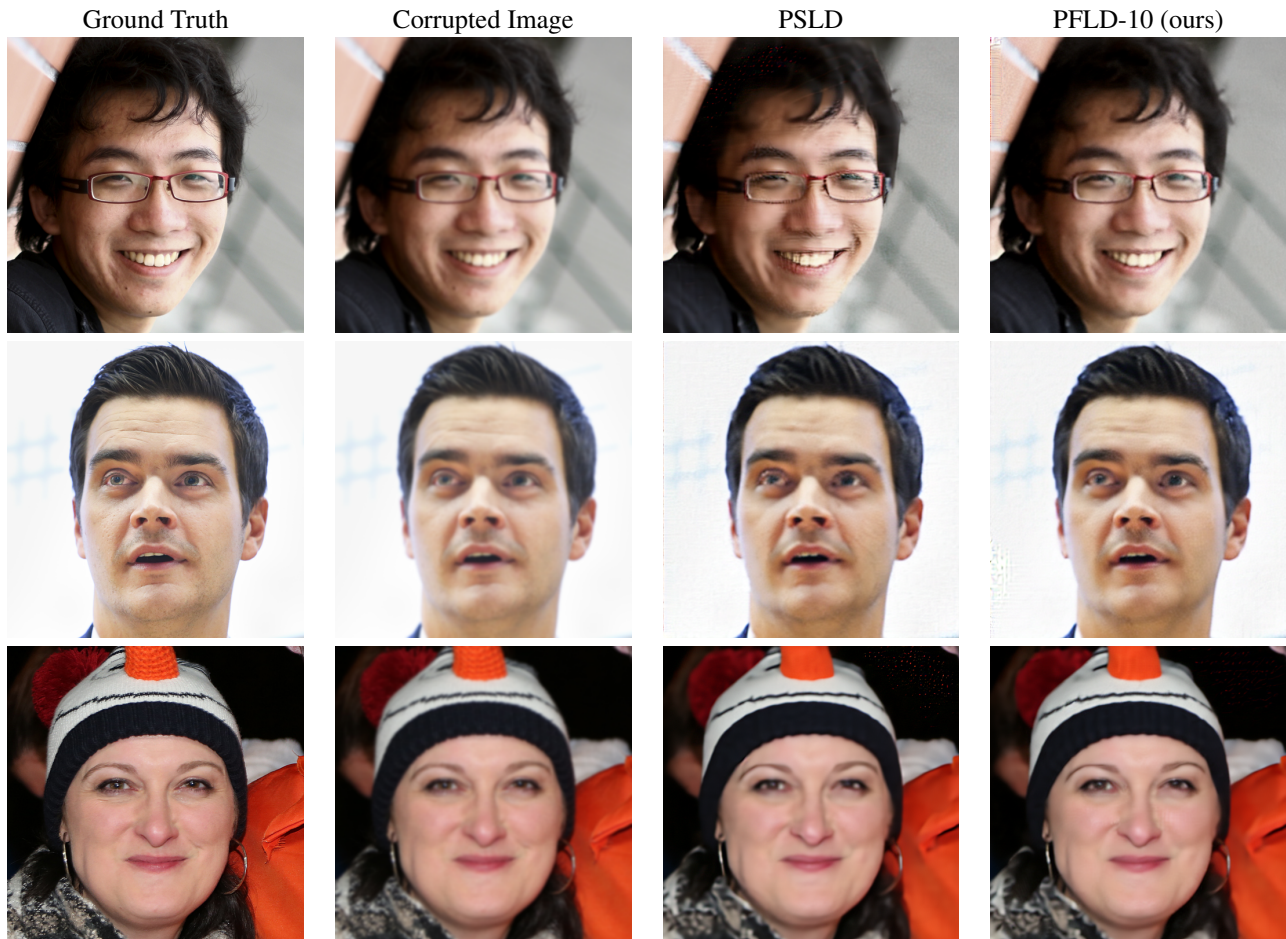


Figure 12: Qualitative results for the Gaussian deblurring task on the FFHQ-1K ( $512 \times 512$ ) dataset. For all samples presented, PFLD-10 produces outputs that are slightly closer to the ground truth. In the first sample, PFLD-10 did not produce an over-sharpened output like PS�D did. In the second sample, the grainy, overly sharp artifacts around the right eyelid of the person are not present in the PFLD-10 output. In the final sample, PFLD-10 reconstructs fine detail around the left eyelid of the subject.